Experimental study of dynamic response of passive flapping hydrofoil in regular wave

Wang, Junxian; Santhosh, Sabin; Colomés, Oriol; Capaldo, Matteo; Yang, Liang

DOI
10.1063/5.0157890

Publication date
2023

Document Version
Final published version

Published in
Physics of Fluids

Physics of Fluids

RESEARCH ARTICLE | JULY 26 2023

Experimental study of dynamic response of passive flapping hydrofoil in regular wave

Special Collection: Recent Advances in Marine Hydrodynamics

Junxian Wang ; Sabin Santhosh ; Oriol Colomés ; Matteo Capaldo ; Liang Yang

Physics of Fluids 35, 077127 (2023)
https://doi.org/10.1063/5.0157890

Physics of Fluids ARTICLE pubs.aip.org/aip/pof

Experimental study of dynamic response of passive flapping hydrofoil in regular wave

Cite as: Phys. Fluids **35**, 077127 (2023); doi: 10.1063/5.0157890
Submitted: 12 May 2023 · Accepted: 10 July 2023 ·
Published Online: 26 July 2023

Junxian Wang,[1] Sabin Santhosh,[1] Oriol Colomés,[2] Matteo Capaldo,[3] and Liang Yang[1,a)]

AFFILIATIONS

[1]Division of Energy and Sustainability, School of Water, Energy and Environment (SWEE), Cranfield University, Bedford MK43 0AL, United Kingdom
[2]Faculty of Civil Engineering and Geosciences, Delft University of Technology, Stevinweg 1, 2628 CN Delft, The Netherlands
[3]TotalEnergies OneTech, Palaiseau, France

Note: This paper is part of the special topic, Recent Advances in Marine Hydrodynamics.
[a)]**Author to whom correspondence should be addressed:** liang.yang@cranfield.ac.uk

ABSTRACT

The hydrofoil harnesses wave energy and converts it into thrust. In this paper, we present the results of the first experimental study investigating the dynamic behavior of a fully passive foil with spring-loaded pitch and heave in regular waves. Our study shows that the real-time load signal is multi-harmonic with strong superposition, directly proving the robust energy harvesting performance due to the restoring springs. By interpreting the hydrofoil's pose and path from an image sequence captured underwater, we conclude the dynamic evolution of the fully passive hydrofoil interacting with regular waves. The hydrofoil's dynamics exhibit asymmetric surge, pitch, and heave in a motion cycle. Furthermore, we employ a pixel capturing algorithm with self-correction utility to quantify the hydrofoil's forward displacement from the image sequence of the moving carriage. These findings provide valuable insight into the performance and potential of hydrofoils for marine propulsion.

I. INTRODUCTION

Motivated by birds and fish, research on foil-like structures indicates that oscillating motion can generate thrust.[1,2] Meanwhile, an oscillating foil can extract wave energy[3] and convert it to wave propulsion,[4] which could potentially replace traditional propellers, enhance ship stability by significantly decreasing pitch and heave motion, and reduce ship resistance against waves.[5,6] A flapping activity denotes that the foil undergoes a combined motion (i.e., heave and pitch). Investigation of a flapping foil has three different arrangements, namely fully active, semi-passive, and fully passive, as shown in Fig. 1, where the double arrow represents active motion. For the present study, a fully passive foil was experimentally tested to reveal its dynamic behavior in regular waves.

The fully passive foil[7] denotes that the heaving and pitching motion are entirely induced by the oncoming flow, which typically employs separate springs for heave and pitch to provide restoring force, while a semi-passive mode[8,9] has only one spring-dominated degree of freedom. Regarding the investigation of passive foils, the addition of a spring system has been confirmed to help generate higher thrust[10] and exhibit excellent behavior in power conversion.[11]

The spring stiffness significantly affects the hydrofoil's dynamic performance. Multi-harmonic signals were detected via spectral analysis of motion responses.[12,13] The pitch angle or flapping amplitude directly displays the passive pitch foil's dynamic motion, which is found to decrease as the spring stiffness becomes larger.[10,14–16] As major parameters that reveal the foil's propulsion performance, the angle of attack, thrust coefficient, and advance speed are shown to relate to spring stiffness, and, more specifically, an optimal stiffness exists to maximize performance.[10,14,15] In addition, the foil's dynamic mechanism, including motion trajectory,[14] within a period was comprehensively analyzed.[16] For the experimental study about foil and wave interaction, there were fixed[17] foils or semi-passive[18] foils attaching underneath the ship to experimentally investigate the impact of foils on ship performance. However, there are very few experimental investigations on the interaction between a fully passive foil and waves. Isshiki and Murakami[19,20] performed experiments on a submerged fully passive foil in regular waves, taking into account the spring stiffness (especially heave spring) and wavelength, and concluded valuable results, including trends in advance speed, thrust, heave, and pitch amplitude.

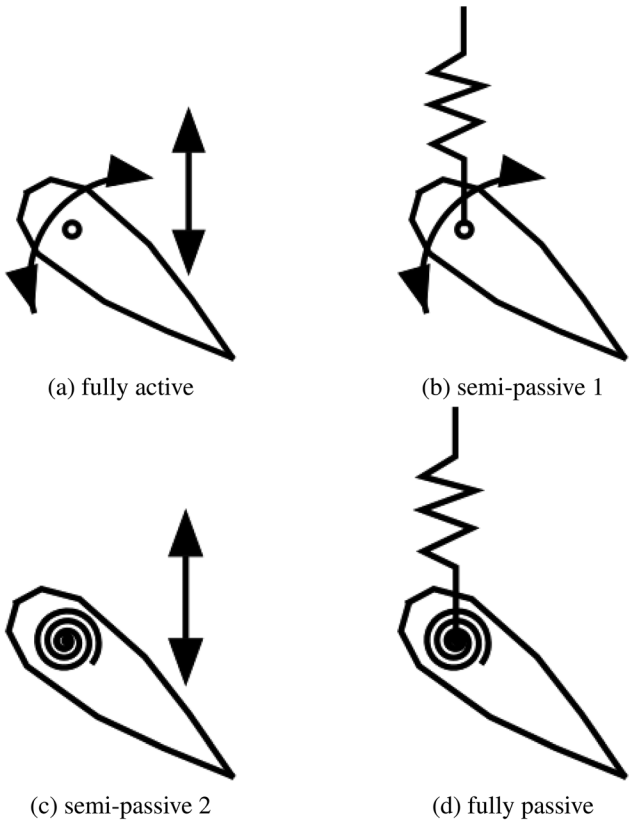

FIG. 1. Schematic sketch of (a) fully active motion, (b) and (c) semi-passive motion, and (d) fully passive motion.

It should be noted that most of the above-mentioned investigation on stiffness effect is based on semi-passive foil. In addition, there are still fundamental issues regarding the interaction between waves and fully passive foils that need to be considered. First, the extension and compression of the spring affects the statistical analysis of thrust (e.g., time-averaged thrust), and the induced variation of force time series is also worthy of investigation. In comparison to semi-passive foils,[12,13] the spring stiffness investigation based on full passive foils needs further investigation, particularly in relation to force and advance speed. In addition, the complicated induced motion of the fully passive hydrofoil, which includes surge, heave, and pitch, has not been experimentally studied before and is thus worth exploring.

The present study conducted experiments on a fully passive hydrofoil subjected to fixed regular waves with varying pitch spring stiffness. Real-time thrust and drag loads were collected and analyzed to reveal the impact of restoring springs on energy harvesting enhancement. The hydrofoil's underwater pose and path within a cycle were discussed, leading to a summary of dynamic pose and path of fully passive hydrofoils interacting with regular waves. Additionally, the "pixel capturing" method with self-correction was used to quantitatively describe the forward displacement. The results of this study provide a deeper understanding of the response of fully passive hydrofoils to regular waves. Analysis on the hydrofoil's dynamic motion helps reveal a deeper understanding of its motion mechanism. Furthermore, the present investigation into the spring effect has the potential to make a substantial contribution toward improving energy conversion efficiency.

II. METHODOLOGY

A. Experimental setup

The present experiments were conducted in an open circulating wave tank,[21] as shown in Fig. 2, maintained at Cranfield University. The tank measures 30 m in length, 1.5 m in breadth, and has a design water depth of 1.5 m. The tank is approximately 1 m above the ground. The piston-type wave generator, located near one end of the tank, can produce various regular and irregular waves, with a maximum wave height of 0.28 m. The test section of the tank is located in the middle, approximately 8.4 m downstream of the wave paddle. A wave absorber and an absorption beach are installed at the two ends of the wave flume to dissipate wave energy and reduce wave reflection. The circulating water undergoes regular UV (ultraviolet) disinfection to ensure high-quality transparency. Additionally, the towing facility over the wave tank can generate towing speeds of up to 2.5 m/s.

Referring to Isshiki and Murakami,[19,20] the present 3D hydrofoil model employs a symmetric NACA0024-type foil (Table I) with its dimensions scaled down to a chord length (c) of 0.2 m and a span length (b) of 0.1 m, as shown in Fig. 3(b). The chord line has two pivot points, one (P1) located 25 mm after the leading edge (A), and the other (P2) located 20 mm ahead of the trailing edge (B). Two "V"-shaped slots [see Fig. 3(a)] are located in the middle span around the pivot points to allow rods to pass through. It should be noted that the small aspect ratio (i.e., b/c) of the present model leads to three-dimensionality of the flow structure in the wake zone, which affects the hydrofoil's performance[6] and has been considered and incorporated into the experimental original design. In addition, the blockage ratio was calculated at around 0.2%, suggesting that its impact could be ignored. A hydrofoil digital model with a definition of geometrical parameters was established using Gmsh software (version 4.8.4), and

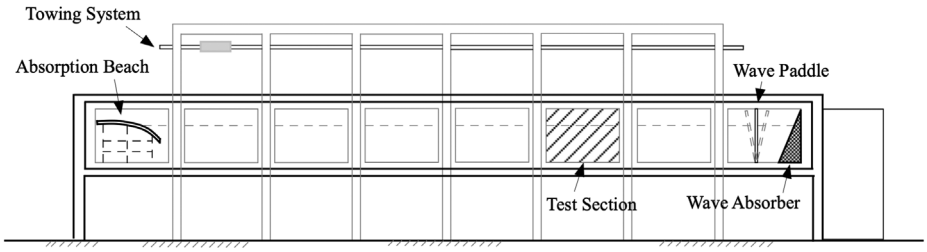

FIG. 2. Schematic sketch of the wave tank at Cranfield University.

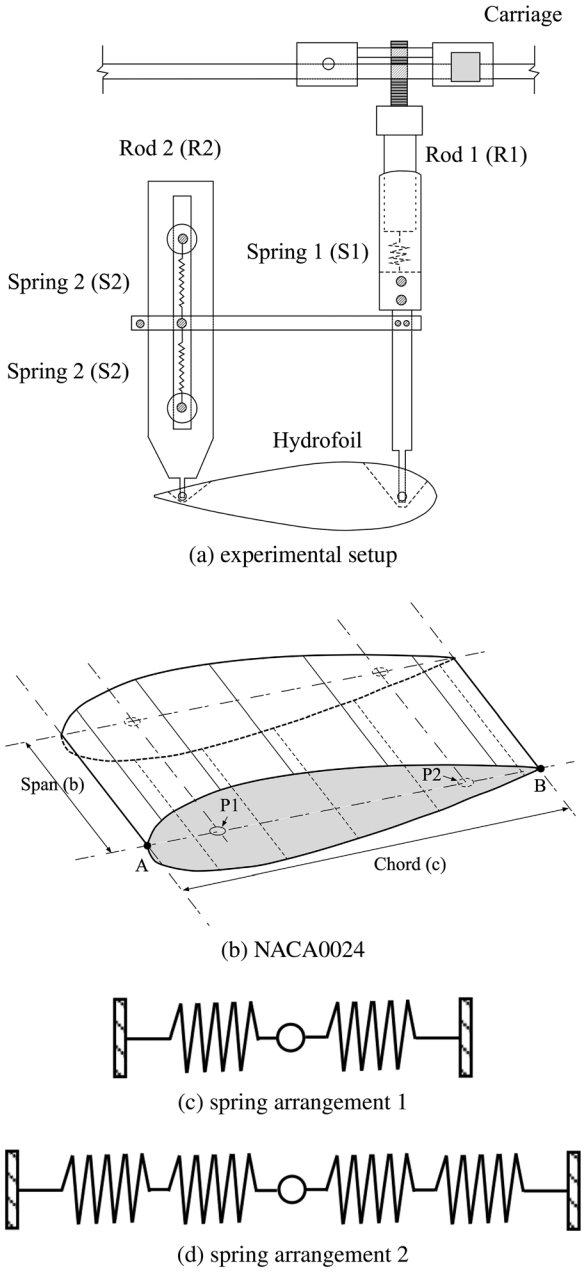

FIG. 3. Schematic sketch: (a) experimental setup, (b) NACA0024 foil, (c) spring arrangement 1, and (d) spring arrangement 2.

then the corresponding output *.stl* file was transferred to a 3D printer (Brand: Ender 5 pro) to create the physical model.

Considering the three degrees of freedom (i.e., surge, heave, and pitch) of the hydrofoil's motion, the experimental setup shown in Fig. 3(a) was designed and constructed. It includes a top carriage, a middle connection consisting of two rods (R1 and R2), restoring springs (S1 and S2), and the submerged hydrofoil model (Table II). A pair of trail (MODEL: SBR16 1000/1500 mm) are placed streamwise over the water and fixed on two aluminum beams spanning the tank. The hydrofoil is connected to R1 and R2 via the pivot joints P1 and P2, respectively. As R1 connects its upper end to the carriage using screws, the carriage (MODEL: SBR16UU) moves forward along the rails (i.e., surge motion) with the hydrofoil underneath it. The inner and outer of R1 are connected to each other via a compression spring (S2) to allow the hydrofoil to move up and down (i.e., heave motion). A horizontal slender plate is fixed at one end to R1, and a pair of extension springs (S1) is installed within the shaft of R2 and related to R2 via the horizontal slender plate to achieve the hydrofoil's trailing edge offset up and down (i.e., pitching motion). As Isshiki and Murakami[20] concluded that the specified restoring force corresponding to heave/pitch motion significantly affects the hydrofoil's motion in the streamwise direction (i.e., surge), the present study chose two extension springs (spring A and B) with different stiffness ($k = 60$ and 130 N/m) and one compression spring (spring C, $k = 490$ N/m) to investigate their impact. According to Hooke's law equation,

$$F = -k\Delta x, \tag{1}$$

where F is the applied load, k is the stiffness, and Δx is the axial change in displacement due to the force. If two identical extension springs are axially connected, the distance variation (Δx) could be doubled subject to the applied load, and, thus, the corresponding actual stiffness could be halved. Note that this study employs the extension spring as "pitch spring" to fulfill the foil's pitch motion. Therefore, one pitch spring arrangement specifies one spring A ($k = 130$ N/m) on each side [Fig. 3(c)], and another setting arranges two identical spring B ($k = 60$ N/m) on each side to achieve an actual stiffness of 30 N/m [Fig. 3(d)]. The initial length of the pitch spring should be properly assigned, as 70 mm for $k = 130$ N/m and 100 mm for $k = 30$ N/m. For this study, we only considered a fixed regular wave with a wave amplitude (A) of 0.05 m and a wave frequency (f) of 0.75 Hz. The water depth is in agreement with the design depth of 1.5 m, and the draft of the hydrofoil (i.e., the distance between the water surface and the symmetry line) is chosen to be approximately 0.1 m. As this work is part of a comprehensive series of experimental testing, we focused on analyzing the physical phenomena by considering only a fixed regular wave condition with two different pitch stiffness values. The subsequent testing has confirmed the reasonableness of the present results. Furthermore, this experiment series includes tests on different springs with a stiffness range from 18 to 300 N/m, and these two selected stiffness values were considered representative.

B. Data collection and post-processing

The main experimental objective was to measure the real-time load generated by the hydrofoil, record the underwater pose evolution of the hydrofoil, and track the top carriage's real-time displacement. To measure the force, a multi-functional "Go Direct®" sensor was used with a measuring range of ±50 N and a minimum scale of ±0.1 N. A high-definition camera with a resolution of "1920 × 1080 pixel"[2] was employed to film the hydrofoil and the carriage. It is worth noting that experiments involving each pitch spring stiffness were repeated three times to independently measure the force and film the hydrofoil and carriage. Figure 4 provides a detailed illustration of the experimental arrangement during the measurement of force and displacement.

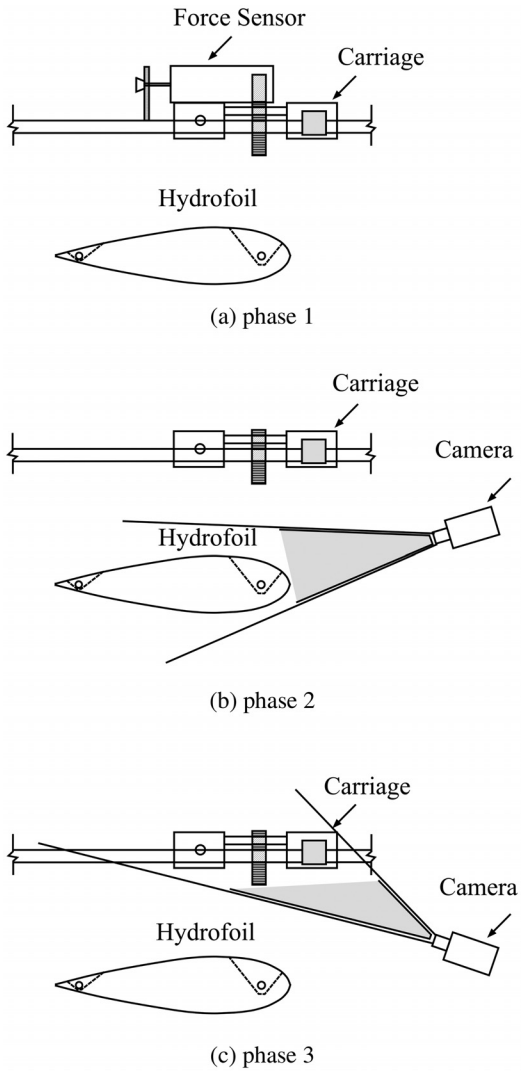

FIG. 4. Experimental arrangement for the pitch spring stiffness $k = 130$ and 30 N/m for different phases: (a) phase 1, (b) phase 2, and (c) phase 3.

During phase 1, the carriage, together with the force sensor, was fixed on the trail to measure the force. Then, the force sensor was removed, and the carriage was allowed to move freely during phase 2 while the camera recorded the hydrofoil response from the side of the wave tank. Finally, during phase 3, the experiment was repeated with the carriage running freely, and the camera placed on top of the wave tank's sidewall recorded the top carriage motion.

For data post-processing, we employed force spectral analysis using the discrete Fourier transform (DFT) method. Additionally, we implemented phase-averaging techniques to precisely evaluate load variation over one cycle. Furthermore, the core mathematical approach for tracking carriage motion is to calculate the two-dimensional cross correlation coefficient between two successive film captures.

III. RESULTS AND DISCUSSION

In accordance with the arrangement in Fig. 4, experiments were carried out at fixed regular wave of $A = 0.05$ m and $f = 0.75$ Hz. The spring stiffness was $k = 30$ and 130 N/m for pitch and $k = 490$ N/m for heave. The related outcome contains time series of load, image sequence of hydrofoil's pose and position, and image sequence of moving carriage. These reveal the following: (1) the periodic load and its dependence on waves and springs; (2) a complete cycle of the hydrofoil's transient behavior; and (3) the relationship between spring stiffness and the advance speed.

A. Harmonic loads

A total of 30-s stable load signals, approximately 40 loops, were selected for all cases studied, 5 s of which were plotted in Figs. 5(a) and 5(b), corresponding to the pitch spring stiffness values of $k = 130$ and 30 N/m, respectively. Note that dashed lines connect local maxima/minima to mark the trend. The above two figures show that the force varies periodically over time, with the duration of three complete cycles in Fig. 5(a) being 1.32, 1.34, and 1.34 s, equal to the applied wave period. This indicates that the load is directly dependent on the oncoming wave. As positive force and negative force denote thrust and drag, respectively, load variation within a cycle directly reveals the thrust-drag transition for regular wave and fully passive hydrofoil interaction, which was numerically observed by Xing *et al.*[22] The time series in Figs. 5(a) and 5(b) shows a clear positive mean value, indicating that the thrust force dominates throughout the process, thus resulting in the observed slow drift in Fig. 9. However, the averaged maximum thrust and drag from the three presented cycles are 1.13 N and 1.89 N for $k = 130$ N/m and 1.85 N and 1.12 N for $k = 30$ N/m. This shows that pitch stiffness affects the load generated by the hydrofoil, and more specifically, stiffness changing from 130 to 30 N/m could increase thrust and reduce drag. It can also be seen in Figs. 5(a) and 5(b) that each cycle contains several fluctuations at different magnitudes, indicating the occurrence of signal superposition. Feng *et al.*[12] found signal superposition via numerical simulation on a semi-passive foil. However, compared to that from a semi-passive foil, the present experimental result displays superposition with a larger magnitude, which infers that the restoring spring gives rise to signal superposition and a fully passive mode with heave and pitch spring enhances the superposition magnitude.

The corresponding spectral analysis in Figs. 5(e) and 5(f) reveals harmonics, including the shared dominant frequency of 0.75 Hz (equal to wave frequency) and the outstanding fifth harmonic (3.76 Hz) for $k = 130$ N/m and the fourth harmonic (3 Hz) for $k = 30$ N/m. In addition, higher-harmonic frequency still turns up (times of the excitation frequency) when the wave frequency changes to 0.85 and 1 Hz, indicating its existence independent from the system natural frequency. The harmonic frequency was also found by Feng *et al.*[12] and Wang *et al.*[13] via numerical simulation on semi-passive foil. Subsequently, the original 30-s load signal was phase-averaged, and the output is presented in Figs. 5(c) and 5(d). For a specific pitch spring stiffness [e.g., 30 N/m in Fig. 5(d)], hollow squares and triangles represent the peaks of local thrust and drag, which follow linear changing trends at different rates, respectively. The small fluctuations within one cycle have been proven to be due to the heave/pitch spring. Furthermore, the utilized spring system can be regarded as a "power takeoff" module. As

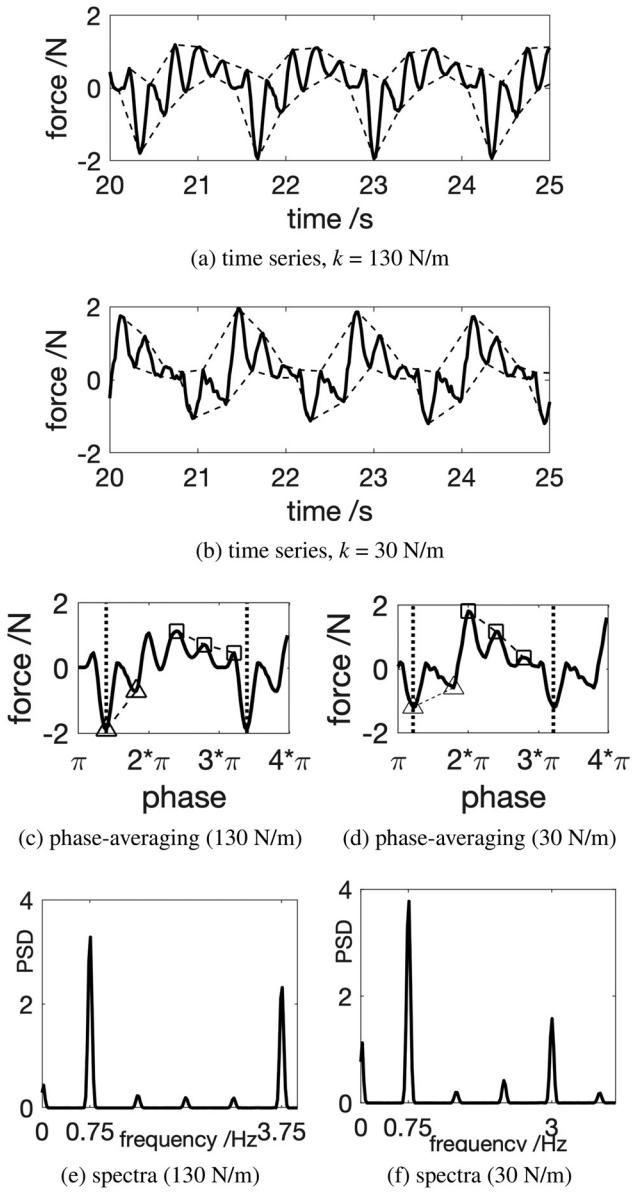

FIG. 5. (a) Time series of load variation for the pitch spring stiffness $k = 130$ N/m, (b) time series of load variation for the pitch spring stiffness $k = 30$ N/m, (c) phase-averaging of load variation for the pitch spring stiffness $k = 130$ N/m, (d) phase-averaging of load variation for the pitch spring stiffness $k = 30$ N/m, (e) spectra of load variation for the pitch spring stiffness $k = 130$ N/m, and (f) spectra of load variation for the pitch spring stiffness $k = 30$ N/m.

Boudreau *et al.*[11] proved, fully passive foils can have good behavior for converting power, and the "small fluctuations" of the present load signals clearly describe the restoring spring's mechanism, which provides direct proof of higher power conversion of a fully passive foil in regular waves. The compression and extension process of the spring is accompanied by energy storage and release, which means more energy is extracted from the wave and converted to propulsion. In addition, the comparison of Figs. 5(c) and 5(d) shows that reducing stiffness from 130 to 30 N/m causes larger thrust, resulting in better propulsion performance.

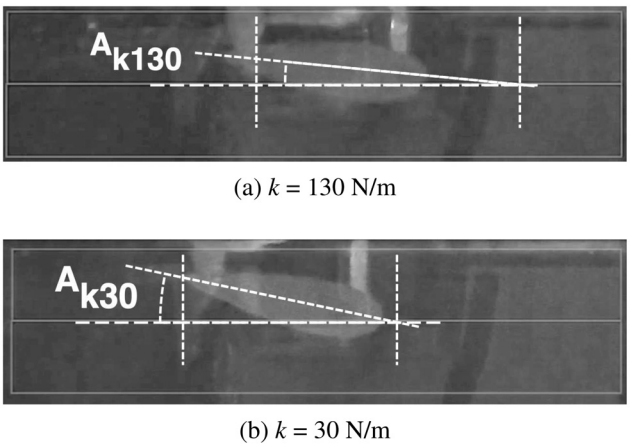

FIG. 6. Hydrofoil pose and flapping angle for (a) $k = 130$ and (b) 30 N/m.

B. Dynamic pose and path

Image sequence of hydrofoil underwater motion at a constant interval of 0.1 s was obtained via the phase 2 experiments with a free running carriage and different pitch spring ($k = 30$ and 130 N/m). Two representative image captures in Figs. 6(a) and 6(b) were chosen to interpret the maximum flapping angle for $k = 130$ and 30 N/m. The flapping angle (marked as A_{k130} and A_{k30}) denotes the angle between chord line and the horizontal line. It can be observed that the flapping angle for $k = 30$ N/m is significantly larger than that of $k = 130$ N/m, evidencing that larger pitch spring stiffness for a fully passive foil could suppress the flapping magnitude, which is in agreement with results from semi-passive foil.[16] Considering the fact that Strouhal number determines thrust generation[23] and is calculated using flapping magnitude or angle, it can be concluded that the pitch stiffness affects the flapping angle and, consequently, the load generated by the hydrofoil.

Subsequently, a total of 14 successive captures [Figs. 7(a)–7(n)] for $k = 30$ N/m were presented to describe the hydrofoil's dynamic motion within a complete cycle. The schematic sketch in Fig. 7(o) displays one complete wave elevation cycle. Location A and E correspond to Figs. 7(a) and 7(n) due to the identical water surface elevation (i.e., trough). Similarly, Figs. 7(b)–7(d), 7(e)–7(g), 7(h)–7(j), and 7(k)–7(m) represent four quarters of the wave cycle, corresponding to the AB, BC, CD, and DE parts in Fig. 7(o). In Fig. 7(a), the hydrofoil is located

TABLE I. NACA0024 model[a] dimension.

Property	Value (m)	Property	Value (m)
Span length (b)	0.1	AP_1	0.025
Chord length (c)	0.2	P_2B	0.02
P_1P_2	0.155		

[a]Material: PLA.

TABLE II. Detailed information of the experimental setup.

Property	Dimension/stiffness	Material	Comment
Carriage	$0.12 \times 0.212 \times 0.034\,\mathrm{m}^3$	Aluminum	Hexahedron
Rod 1 (R1)	$0.038 \times 0.62\,\mathrm{m}^2$	PLA	Cylinder
Rod 2 (R2)	$0.0015 \times 0.05 \times 0.41\,\mathrm{m}^3$	Aluminum	Thin plate
Spring 1 (S1)	$k = 490$ N/m	Steel	Compression
Spring 2 (S2)	$k = 60$ and 130 N/m	Steel	Extension

in its balance position. In Figs. 7(b)–7(d), the hydrofoils lift upward, and the amplitude of the offset of the trailing edge gradually increases. For the horizontal direction, the hydrofoil moves forward at a small distance in Figs. 7(b) and 7(c) and then moves back in Fig. 7(d). For the next quarter, the hydrofoil moves downward and returns to the original balance position in Fig. 7(g) (i.e., location C). In the third quarter [Figs. 7(h)–7(j)], the hydrofoil strokes downward with chord line pointing upward, and, at the same time, it makes a significant advance displacement. Subsequently, in the last quarter cycle, the hydrofoil flaps back to the balance position as well as makes another huge forward displacement. More details can be obtained if we discuss it together with the wave elevation. The front side of the wave lifts the water level, causing the hydrofoil to flap upward, and the rear side of the wave causes the hydrofoil to flap downward. However, the hydrofoil only makes a significant advance displacement in the rear side of the wave, indicating that the hydrofoil and restoring springs extract and store wave energy for the front side of the wave and convert it to propulsion after the wave crest.

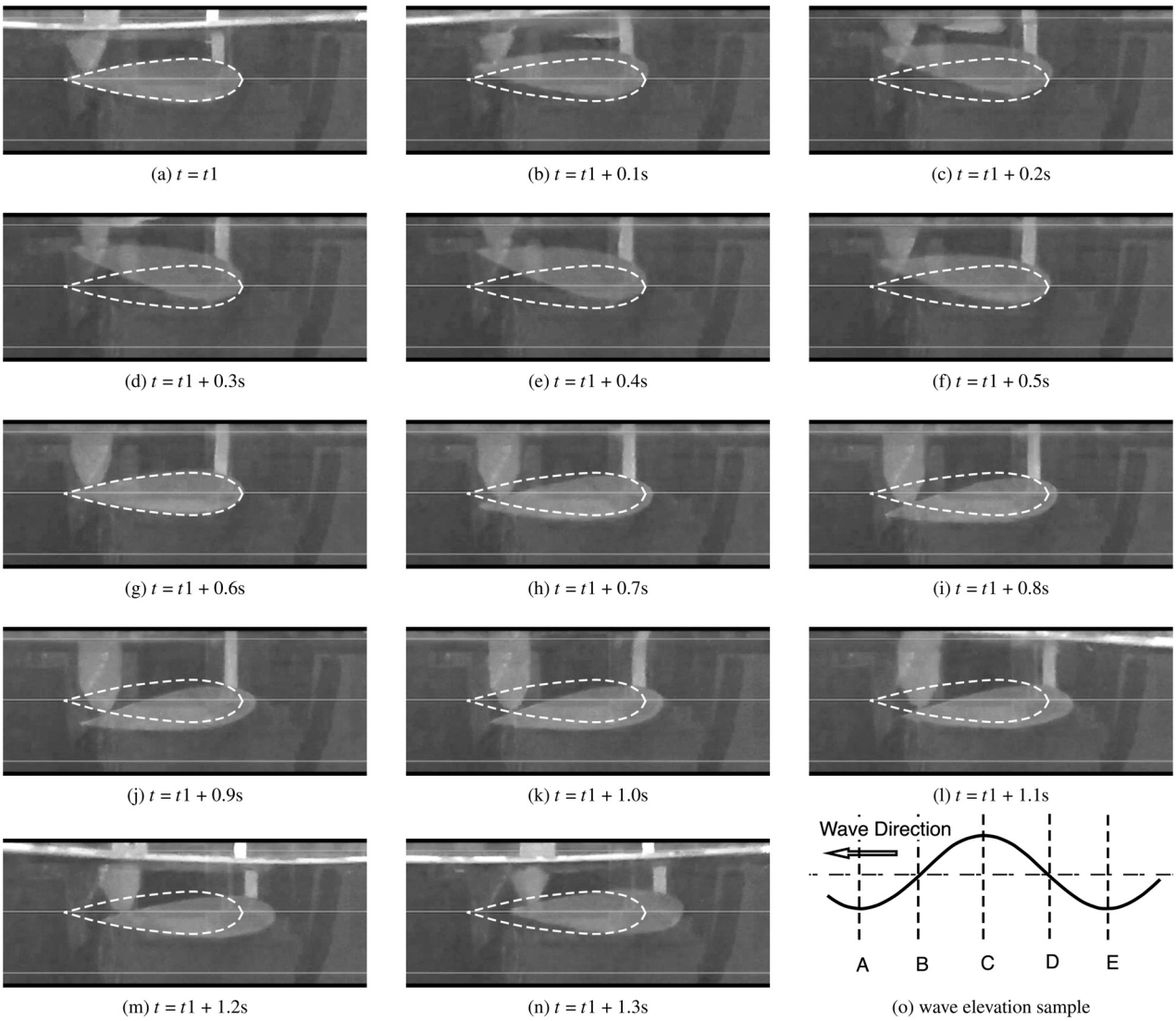

FIG. 7. (a)–(n) A complete cycle of hydrofoil underwater motion for $k = 30$ N/m with time interval 0.1 s and (o) wave elevation sample.

According to the discussion regarding Fig. 7, a sketch collection was summarized and illustrated in Fig. 8 to describe the pose evolution and path line of a fully passive hydrofoil in regular waves. The dynamic process consists of two stages, differing in surge, pitch, and heave motion. It is worth noting that the bold-marked foil denotes the initial pose, and the foil poses (P1–P7) are ordered. Poses 1–4 describe the first stage when the hydrofoil starts from a balance position, then shifts and flaps upward, and return to the identical balance position. For the second stage (i.e., poses 4–7), the hydrofoil diverts downward with a smaller offset and flaps downward at a smaller scale flapping magnitude, accompanied by significant advance displacement. More specifically, the dynamic process reveals the unique features of the fully passive foil dynamic response, including the "forth-and-back" surge component, the asymmetrical flapping angle (i.e., pitch), and the asymmetrical offset (i.e., heave). Linear wave theory states that a fluid particle below the surface moves along a closed orbit. Consequently, the hydrofoil's forth-and-back surge response might be attributed to this orbital motion. Moreover, the diameter of the orbit changes as the fluid particle descends, which could help explain the aforementioned asymmetrical flapping angle and offset. For the comparison, a semi-passive foil was found to keep propulsion force component, indicating advance movement throughout one period,[14] and the maximum pitch angle of flapping up and down is the same.[16] Considering the relation with wave elevation, the first stage and second stage mainly take place in the front and rear sides of the wave, respectively.

C. Advance speed via pixel capturing

The third experimental part filmed the carriage displacement and obtained similar trend in terms of different pitch stiffness ($k = 130$ and 30 N/m). Consequently, Figs. 9(a)–9(d) are captures about moving carriage at pitch stiffness of 30 N/m, indicating a huge forward movement within 1.2 s. Specifically, setting the original position (marked as a dashed rectangle) as a reference, the carriage was observed to follow an "onward-backward-onward" path in the middle two moments [Figs. 9(b) and 9(c)], confirming the "thrust-drag" transition. For a quantitative description, the obtained recording was converted into an image sequence at a time interval of 0.2 s. Each pixel corresponds to a grayscale value from 0 to 255, and the image sequence was mathematically expressed as a group of grayscale matrix. The carriage position of all images then can be accurately recognized using cross correlation analysis between two successive images. It should be noted that the ratio of physical distance to pixel difference varies at different area in an image due to "distortion." The term distortion refers to the variation in the ratio of "pixels" to "distance" at different areas in the image, caused by the physical distance variation between the lens and different locations on the track. The "black circle" and "black square" on the carriage are tracked independently to correct the carriage position.

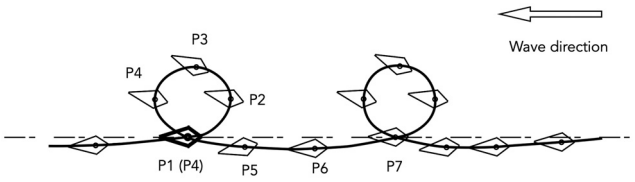

FIG. 8. Sketch collection of fully passive foil in regular wave.

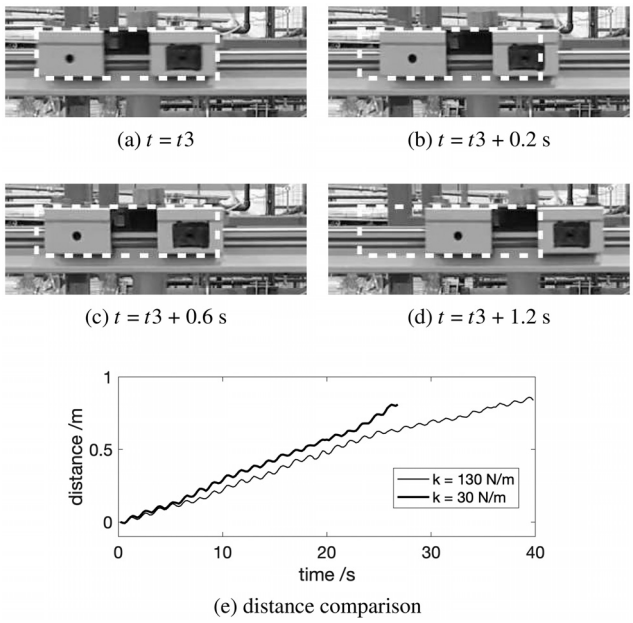

FIG. 9. (a)–(d) Film captures of moving carriage for $k = 30$ /m at $t = t3$, $t3 + 0.2$ s, $t3 + 0.6$ s, and $t3 + 1.2$ s and (e) displacement of carriage against time for $k = 130$ and 30 N/m.

To reduce time consumption, another window containing the carriage was defined for cross correlation calculation, and the window location was updated according to carriage position.

Figure 9(e) compares the advance movement at different pitch spring stiffness. The displacement increases linearly with time, and the local periodic fluctuation coincides with the aforementioned onward-backward-onward path. The result also confirms that the pitch spring stiffness affects the advance displacement. The variation of displacement against time is in agreement with the numerical results from Xing *et al.*[22] A similar trend in advance speed (displacement) was observed for a semi-passive foil.[15]

IV. CONCLUSION

The present experimental study investigates the interaction between a fully passive hydrofoil (spring-loaded at heave and pitch) and regular waves, with a focus on the thrust force, hydrofoil's pose, path, and advance displacement. The regular wave was maintained at a fixed wave height of 0.1 m and frequency of 0.75 Hz, while the pitch spring stiffness was varied at $k = 130$ and 30 N/m. Based on the experimental findings, the following conclusions can be drawn:

- The load varies periodically at the wave frequency. Lower stiffness (e.g., $k = 30$ N/m) leads to a larger thrust and a smaller drag. The time series of the load is harmonic due to the heave and pitch springs. Small fluctuations can be considered to improve energy harvesting.
- The pitch stiffness affects the hydrofoil's pose, with higher stiffness (e.g., $k = 130$ N/m) leading to a smaller flapping angle. We propose the dynamic process of pose and path for a fully passive hydrofoil in regular waves. The surge, pitch, and heave responses differ between the two stages of a complete motion cycle.

- The hydrofoil's advance displacement is analyzed by applying a pixel capturing technique to an image sequence of the moving carriage, revealing an overall linear increasing trend with local fluctuations.

ACKNOWLEDGMENTS

This work was supported by the Department for Transport's (DfT) Transport Research and Innovation Grants (TRIG): G-TRANSPORT: greening transportation of cargo ships via hybrid wave propulsion and UK–Saudi Challenge Fund from British Council: Feasibility study of hybrid propulsion for unmanned surface vehicle for environmental monitoring.

AUTHOR DECLARATIONS

Conflict of Interest

The authors have no conflicts to disclose.

Author Contributions

Junxian Wang: Data curation (equal); Formal analysis (equal); Investigation (equal); Validation (equal); Visualization (equal); Writing – original draft (equal). **Sabin Santhosh:** Data curation (equal). **Oriol Colomés:** Supervision (equal); Writing – review & editing (equal). **Matteo Capaldo:** Validation (equal); Writing – review & editing (equal). **Liang Yang:** Conceptualization (equal); Funding acquisition (equal); Methodology (equal); Project administration (equal); Resources (equal); Supervision (equal).

DATA AVAILABILITY

The data that support the findings of this study are available from the corresponding author upon reasonable request.

REFERENCES

[1]R. Knoller, "Die gesetzedes luftwiderstandes," Flug. Motortech. **3**(21), 1–7 (1909).
[2]A. Betz, "Ein beitrag zur erklaerung segelfluges," Z. Flugtech. Motorluftschiffahrt **3**, 269–272 (1912).
[3]T. Y. T. Wu, "Extraction of flow energy by a wing oscillating in waves," J. Ship Res. **16**(01), 66–78 (1972).
[4]H. Isshiki, "A theory of wave devouring propulsion (1st report) thrust generation by a linear wells turbine," J. Soc. Nav. Archit. Jpn. **1982**, 54–64.
[5]E. Bøckmann and S. Steen, "Model test and simulation of a ship with wave-foils," Appl. Ocean Res. **57**, 8–18 (2016).
[6]X. Wu, X. T. Zhang, X. L. Tian, X. Li, and W. Y. Lu, "A review on fluid dynamics of flapping foils," Ocean Eng. **195**, 106712 (2020).
[7]L. Duarte, N. Dellinger, G. Dellinger, A. Ghenaim, and A. Terfous, "Experimental investigation of the dynamic behaviour of a fully passive flapping foil hydrokinetic turbine," J. Fluids Struct. **88**, 1–12 (2019).
[8]J. Wu, Y. L. Qiu, C. Shu, and N. Zhao, "Pitching-motion-activated flapping foil near solid walls for power extraction: A numerical investigation," Phys. Fluids **26**(8), 083601 (2014).
[9]M. Boudreau, K. Gunther, and G. Dumas, "Free-pitching flapping-foil turbines with imposed sinusoidal heave," J. Fluids Struct. **90**, 110–138 (2019).
[10]E. Bøckmann and S. Steen, "Experiments with actively pitch-controlled and spring-loaded oscillating foils," Appl. Ocean Res. **48**, 227–235 (2014).
[11]M. Boudreau, G. Dumas, M. Rahimpour, and P. Oshkai, "Experimental investigation of the energy extraction by a fully-passive flapping-foil hydrokinetic turbine prototype," J. Fluids Struct. **82**, 446–472 (2018).
[12]Z. X. Feng, Z. Y. Chang, C. Deng, L. Zhao, J. Chen, J. K. Zhang, and Z. Q. Zheng, "Effects of nonlinearity of restoring springs on propulsion performance of wave glider," Nonlinear Dyn. **108**(3), 2007–2022 (2022).
[13]Z. Wang, L. Du, J. S. Zhao, and X. F. Sun, "Structural response and energy extraction of a fully passive flapping foil," J. Fluids Struct. **72**, 96–113 (2017).
[14]Z. Y. Chang, Z. X. Feng, C. Deng, L. Zhao, J. K. Zhang, Z. Q. Zheng, and Z. J. Yu, "Analysis of propulsion performance of wave-propelled mechanism based on fluid-rigid body coupled model," Proc. Inst. Mech. Eng., Part M **236**(3), 713–725 (2022).
[15]H. Q. Sang, G. Liu, X. J. Sun, C. Li, L. Wang, and L. W. Wang, "Hydrodynamic performance analysis of flapping hydrofoil for single-body architecture wave glider," Ocean Eng. **261**, 112118 (2022).
[16]N. Thaweewat, S. Phoemsapthawee, and V. Juntasaro, "Semi-active flapping foil for marine propulsion," Ocean Eng. **147**, 556–564 (2018).
[17]E. Bøckmann and S. Steen, "The effect of a fixed foil on ship propulsion and motions," in *Proceedings of the Third International Symposium on Marine Propulsors* (Australian Maritime College, University of Tasmania, 2013), Vol. 13, pp. 553–561.
[18]J. A. Bowker and N. C. Townsend, "Evaluation of bow foils on ship delivered power in waves using model tests," Appl. Ocean Res. **123**, 103148 (2022).
[19]H. Isshiki and M. Murakami, "A theory of wave devouring propulsion (3rd report) an experimental verification of thrust generation by a passive-type hydrofoil propulsor," J. Soc. Nav. Archit. Jpn. **1983**, 118–128.
[20]H. Isshiki and M. Murakami, "A theory of wave devouring propulsion (4th report) a comparison between theory and experiment in case of a passive-type hydrofoil propulsor," J. Soc. Nav. Archit. Jpn. **1984**, 102–114.
[21]N. Mailh, "Experimental investigation of lift and drag on the NACA 4412 near the water surface," Ph.D. thesis (Cranfield University, 2017).
[22]J. R. Xing, D. Stagonas, P. Hart, C. C. Zhang, J. H. Yang, and L. Yang, "Wave induced thrust on a submerged hydrofoil: Pitch stiffness effects," arXiv:2209.05551 (2022).
[23]D. A. Read, F. S. Hover, and M. S. Triantafyllou, "Forces on oscillating foils for propulsion and maneuvering," J. Fluids Struct. **17**(1), 163–183 (2003).